Caving 2022 - Y Potvin (ed.)

doi:10.36487/ACG_repo/2205_15

A probabilistic evaluation of the displacement-based ground support design approach

R Lowther *Newcrest Mining Limited, Australia*

J De Ross *Newcrest Mining Limited, Australia*

C Orrego *Newcrest Mining Limited, Australia*

D Cuello *DC Geotech, Australia*

Abstract

This paper describes the use of Monte Carlo simulations to perform a probabilistic evaluation of the displacement-based dynamic ground support design methodology used to determine the dynamic ground support requirements for hard rock and brittle behaviour in a high stress environment such as Cadia East. The design approach uses several probabilistic inputs including stress level, depth of strainbursting, bulking time, pre-existing bolt head displacement, rock mass bulking, and peak ground velocity. The main mechanism under consideration is the dynamically loaded strainburst where a remote seismic event triggers a strainburst at an excavation. Several of the inputs are represented as probabilistic distributions to capture the variability and uncertainties within each parameter. The outputs are represented as probabilities of having Factor of Safety less than one for the specific support designs assessed. The methodology defines the acceptance criteria of a given ground support profile based on the layers of protection assessment. An example is detailed where three dynamic ground support systems are assessed for an undercut drill drive using the method.

Keywords: *probabilistic, displacement-based, dynamic ground support, layers of protection assessment*

1 Introduction

This paper demonstrates the application of the probabilistic displacement-based approach to determine a suitable dynamic ground support system to contain strainbursting mechanisms at Cadia. The paper provides details on the displacement-based methodology, the probabilistic approach used to determine the probabilities of failure for various ground support systems, the layers of protection assessment (LOPA), and the distributions of the input parameters used.

The benefits of this approach include the following:

- The variability of the input data is adequately captured in the calculations.
- A large range of resulting factors of safety are considered to determine the probability of failure of each support profile assessed.
- A range of additional controls are considered in conjunction with the ground support to reduce the probability of a person being exposed to a strainburst event that breaches the ground support.

The paper provides an example of three different ground support profiles assessed using the method for an undercut drill drive (UDD) at Cadia East PC1-2 Expansion Project. The drive is set at a depth of approximately 1,200 m and is in volcaniclastic rocks with an average uniaxial compressive strength of 156 MPa. The stress conditions as specified by the stress level (SL) peak above 0.85 during undercutting.

2 Displacement-based design methodology

The displacement-based approach developed by Kaiser (2020a, 2020b), Kaiser & Moss (2022) and Moss & Kaiser (2022) is an evolution of the approach prescribed in the *Canadian Rockburst Support Handbook* (Kaiser

et al. 1996) and experience gained at Freeport's mining operations. The emphasis of the displacement-based approach is to include both the energy and displacement demand into the design methodology. An important feature of this approach is to consider the pre-existing displacement that the support has experienced prior to sustaining a damaging event. The premise here is that if the support has sustained pre-existing damage, then its capacity has been reduced and the support elements do not possess the original capacity as when first installed.

2.1 Dynamically loaded strainbursts

A fundamental component of the displacement-based approach is the concept that a strainburst at an excavation can be triggered by a remote seismic event. If the stress conditions at the excavation are high but not sufficient to generate a self-initiated strainburst, then a large remote seismic event can add a sufficient dynamic stress increment through the peak ground velocity (PGV) to induce a strainburst at the excavation. If the remote seismic event is sufficiently large, then the event can not only trigger the strainburst at the excavation, but also add additional energy and subsequent damage and bulking to the strainburst. This scenario is known as a dynamically loaded strainburst.

Figure 1 shows a dynamically loaded strainburst. Empirical evidence suggests that dynamically loaded strainbursts occur for remote events exceeding magnitudes of ML > 2 (Morissette et al. 2011, 2012). Such dynamically loaded mechanisms have been observed at Cadia (Lowther 2017).

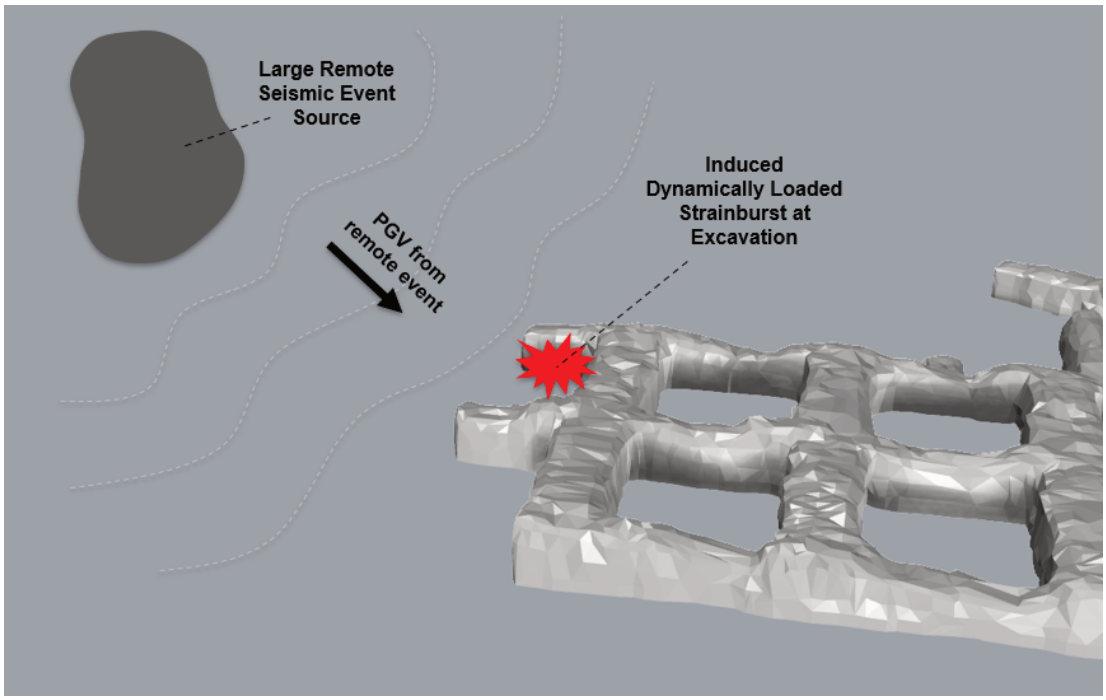

Figure 1 Dynamically loaded strainburst

Figure 2 shows an illustration of the elements associated with a dynamically loaded strainburst with an accompanying photograph of a strainburst event at Cadia East. The illustration highlights the PGV from the remote seismic event, the depth of strainburst (dSB) triggered at the excavation, the dynamic displacement (d_{BF}) and strainburst velocity (v_i) generated from the bulking of the strainburst volume, and the additional depth of fracturing and subsequent bulking (Δd_f) associated with the remote event.

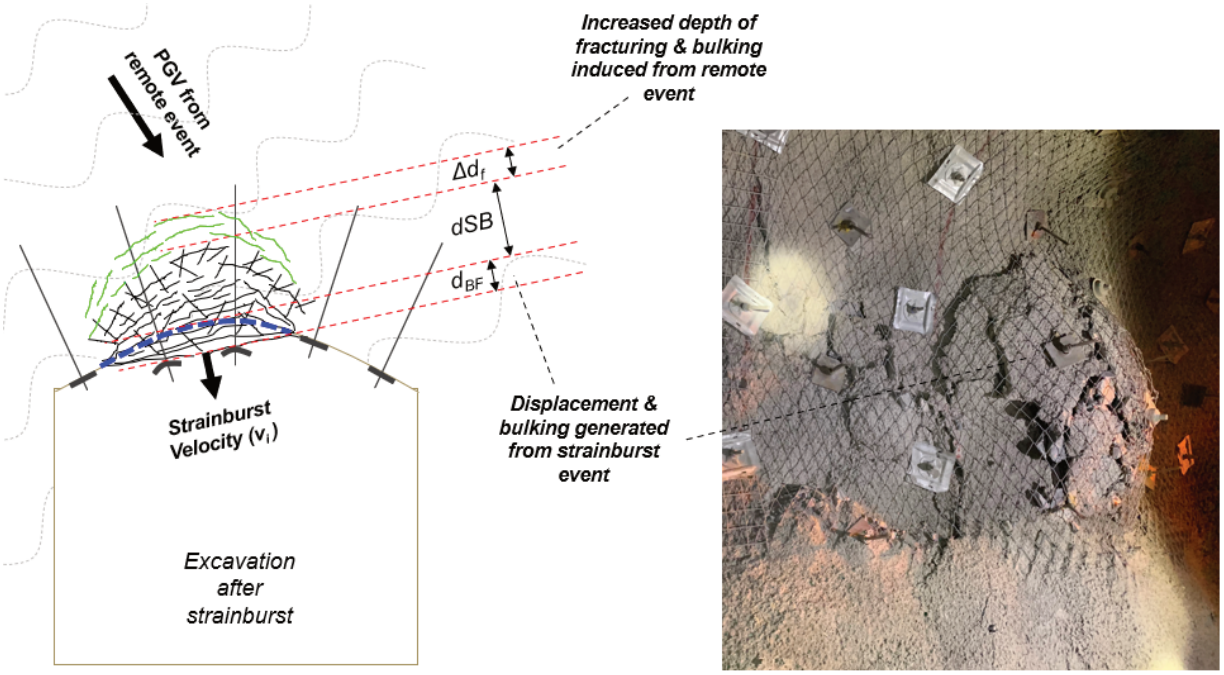

Figure 2 Illustration of a strainburst at an excavation showing the relationship between depth of strainburst (dSB), dynamic displacement (d_{BF}) and the resulting strainburst (bulking) velocity (v_i), and the additional depth of fracturing (Δd_f) associated with the remote event (photo courtesy of J Lett, Cadia, 2022)

2.1.1 Bulking velocity (v_i)

During the strainburst, a fractured volume forms around the excavation, and the rock mass within this volume undergoes sudden bulking due to the lower confinement near the excavation surface. The degree of confinement depends on the distance from the excavation and the density and properties of the installed ground reinforcement and surface support. The depth of the fractured volume is known as the depth of strainburst (dSB) and the amount of bulking that this fractured rock undergoes is governed by the dynamic bulking factor (BF_D). The bulking of the rock mass results in the boundary of the excavation converging inwards and undergoing a displacement which is known as the dynamic displacement (d_{BF}). The dynamic displacement is related to the depth of strainburst and dynamic bulking factor through Equation 1:

$$d_{BF} = dSB \times BF_D \quad (1)$$

where:

dSB = depth of strainburst (m).

BF_D = dynamic bulking factor (%).

The duration of this dynamic displacement is known as the bulking time (t_R) and is measured in milliseconds (ms). The velocity of bulking at the inner face of the burst volume (v_i) as experienced by the surface support and reinforcement elements is a function of the dynamic displacement and the bulking time and is represented by Equation 2.

$$v_i = \left(\frac{d_{BF}}{t_R}\right) \times 1{,}000 \quad (2)$$

where:

v_i = maximum strainburst (bulking) velocity (m/s).

d_{BF} = dynamic displacement (m).

t_R = bulking time (ms).

2.1.2 Strainburst energy

The type of energy associated with a strainburst event at the excavation is kinetic energy. The mass of the strainburst volume is mobilised as the rock undergoes dynamic bulking. An important consideration is that the strainburst velocity varies across the depth of strainburst (dSB). This is because the velocity of the fractured rock at the excavation boundary is the maximum value of v_i, while the velocity of the fractured rock at the back of the strainburst volume where it meets the intact rock is zero. Hence for the strainburst volume, the velocity acting on the entire volume is approximated as the average bulking velocity ($v_i/2$). It is conservatively assumed that the entire depth of strainburst is ejected.

For a dynamically loaded strainburst, the remote event that triggered the strainburst generates a low frequency (typically ≤ 10 Hz) PGV which permeates the entire rock mass containing the excavation. This PGV adds to the energy of the strainburst volume.

The resulting kinetic energy of strainburst volume is defined by the Equation 3:

$$E_{kvi} = \left(\frac{1}{2} \times dSB \times \rho\right) \times \left(\left(\frac{v_i}{2}\right)^2 + (n \times PGV)^2\right) \quad (3)$$

where:

dSB = depth of strainburst (m).

v_i = maximum strainburst (bulking) velocity (m/s).

ρ = rock mass density (t/m^3).

PGV = peak ground velocity of the remote triggering event (m/s).

N = amplification factor = 1 for long wavelengths such that the entire volume is accelerated in one direction.

2.1.3 Dynamically loaded strainburst displacements

A strainburst event not only generates energy, but also bulking displacements. In a dynamically loaded strainburst scenario, the strainburst event generates the dynamic displacement d_{BF} that is due to the rock mass bulking over the depth of the strainburst dSB. The energy from the remote event, however, can also generate an additional depth of fracturing Δd_f with associated bulking. This is because the remote event can cause a dynamic stress increase at the excavation which results in an increase in depth of bursting and subsequent bulking. This additional depth of fracturing can be estimated by the process described by Kaiser et al (1996) or by interrogating extensometer data or observation drill holes at strainburst locations. Figure 2 shows the various zones of displacement generated during a dynamically loaded strainburst event.

The additional displacement (Δdisp) generated by the remote event is determined by applying the dynamic bulking factor (BF_d) to the increase in the depth of fracturing (Δd_f). This additional displacement is determined from Equation 4:

$$\Delta disp = \Delta d_f \times BF_d \times 1{,}000 \quad (4)$$

where:

Δd_f = increase in depth of fracturing due to the remote event (m).

BF_d = dynamic bulking factor (%).

2.1.4 Total displacement demand

The total displacement demand generated by the dynamically loaded strainburst event as measured at the bolt head is simply the sum of the displacement generated by the strainburst event, the displacement generated by the remote event, and the displacement that existed prior to the strainburst occurring.

The total displacement demand is determined from Equation 5:

$$\Sigma disp = d_0 + d_{BF} + \Delta disp \quad (5)$$

where:

d_0 = all types of mining-induced static bolt head displacement (mm) imposed on support before the strainburst (incl. displacements due to drift advance, stress-fracturing, pre-tensioning, etc.).

d_{BF} = dynamic displacement from the strainburst event (mm).

$\Delta disp$ = additional displacement from the remote event (mm).

2.1.5 Remnant capacity of the support elements

During the strainburst event, the support elements which include the rockbolt, cable bolts, and surface support can perform work by deforming and absorbing energy during the process. If the elements are freshly installed, then they can perform work according to their design capacities.

A fundamental component of the displacement-based approach is that if the support elements have already experienced some displacement (d_0) prior to the strainburst event occurring. Their capacity has been reduced because of the displacement and the remnant capacity is less than the installed capacity. This is particularly important in practice because the pre-deformed support may fail at a lower-than-expected demand as its remnant capacity is consumed in the strainburst event.

Figure 3 shows an example of a fresh rockbolt compared to a deformed rockbolt that exhibits a pre-existing displacement d_0. This pre-existing displacement has reduced the bolt's original work capacity, hence its ability to perform work during a strainburst event is less than that of the fresh bolt.

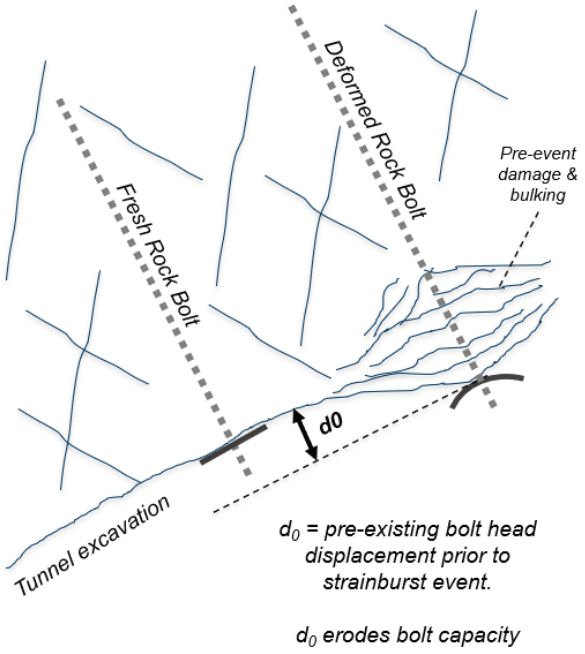

Figure 3 An example of a fresh rockbolt compared to a rockbolt that exhibits pre-existing deformation d_0. This pre-existing deformation has eroded the bolt's capacity to perform work prior to the strainburst event occurring

2.1.6 *Demand path*

The demand path is the energy & displacement demand created by the dynamically loaded strainburst event. The end point of the demand path in the displacement–energy space (Figure 4) is a function of the total energy demand ΣE and total displacement demand Σdisp. The demand path to reach this end point is assumed to be a parabolic shape of order n and is defined by Equation 6:

$$Demand\ Path = \left(\frac{(disp-d_0)^n}{(\Sigma disp-d_0)^n}\right) \times \Sigma E \quad (6)$$

where:

disp = the displacement undergone by the support elements (mm).

d_0 = the pre-existing support element displacement (mm).

Σdisp = the total displacement demand from the event (mm).

ΣE = the total energy demand from the event (kJ/m^2)

n = the order of the demand path parabola; n = 4 was chosen for Cadia operations (Kaiser 2020b).

2.1.7 *Local reinforcement element displacement assessments*

The local reinforcement element displacement assessments consider the Factor of Safety (FoS) for each individual bolt element when subjected to the dynamically loaded strainburst event as opposed to the overall support system. The overall support system capacities can also be assessed. This paper focuses on the assessment of the local reinforcement elements as it is a simpler and more conservative approach. If the overall support system is considered, then the remnant capacities would represent both the bolt elements and the surface support combined.

Figure 4 shows the plot of the demand path for a dynamically loaded strainburst event that occurs after some initial displacement (d_0) has been sustained by the bolts. The plot also shows the remnant capacity of two different bolt types. Bolt Type #1 has a higher installed energy capacity but less ductility (displacement capacity) that Bolt Type #2. The point of failure is denoted by the intersection of the demand path and the remnant capacity. Accordingly, in this example Bolt Type #1 fails whereas Bolt Type #2 is stable.

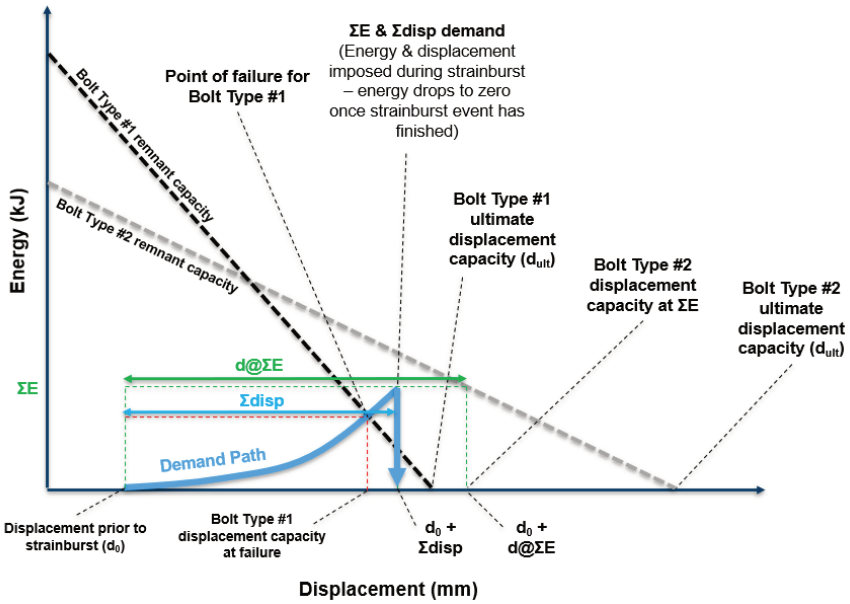

Figure 4 Plot of the demand path for a dynamically loaded strainburst event. The plot shows the demand path in relation to the remnant capacity for two different bolt types (local assessment) and denotes the point at which the demand path causes Bolt Type #1 to fail

The static FoS(disp) directly after the strainburst for this scenario (Equation 7) is the ultimate displacement capacity of Bolt Type #2 minus the initial displacement d_0, divided by the total displacement demand (Σdisp) from the event, resulting in a FoS > 1.0. However, during the strainburst (at the point of maximum energy and displacement demand), the dynamic FoS(disp) is to be measured relative to the remnant displacement capacity at the imposed energy level (d@ΣE), shown by Equation 3. It is much lower than the static FoS(disp) and is unity if the demand path reaches the remnant capacity.

$$Local\ static\ FoS\ (disp) = \frac{dult - d_0}{\Sigma disp} \tag{7}$$

where:

d_{ult} = ultimate displacement capacity of the bolt elements.

d_0 = pre-existing bolt head displacement.

$\Sigma disp$ = displacement demand from the strainburst event.

$$Local\ dynamic\ FoS\ (disp) = \frac{d@\Sigma E}{\Sigma disp} \tag{8}$$

where:

$d@\Sigma E$ = remnant displacement capacity at the imposed strainburst energy.

$\Sigma disp$ = displacement demand from the strainburst event.

If both bolt types were used to support the excavation, then the strainburst event would cause Bolt Type #1 to fail, however Bolt Type #2 would survive and, provided the surface support remains intact, would continue to support the excavation.

By contrast, if the excavation was only supported by Bolt Type #1, then the support element and consequently the surface support would fail. The bolts' energy and displacement capacity at the point of failure is indicated in Figure 4. The best-case scenario here would be that the surface support continues to be supported by adjacent bolts that were not damaged by the strainburst event. Such scenarios are often observed in practice, whereby a single bolt fails but the surface support can bridge over the wider effective bolt spacing. This scenario will lead to a dynamic FoS(disp) < 1.0 for Equation 8.

2.2 Probabilistic approach

The probabilistic approach uses distributions for both the input parameters and the output parameters using a Monte Carlo simulation in Microsoft Excel. The simulation generates 1,000 values for each of the input parameters and then performs 1,000 calculations to generate the distributions for the displacement-based output FoS values considered.

The input parameters consisting of depth of strainburst (dSB), bulking time (t_R) and pre-existing bolt head displacement (d_0) are expressed as triangular distributions utilising the minimum, average, and maximum values of each respective dataset. The PGV input is expressed as a normal distribution utilising a mean and standard deviation derived from the Cadia ground motion prediction equations (Mendecki 2021).

The outputs consisting of the static FoS (disp) and the dynamic FoS (disp) are represented as normal distributions which allow the probabilities of failure (Pf) to be determined. The Pf is simply defined as the percentage of results within the normal distributions where the FoS values are less than 1.0. Figure 5shows the process map for the Monte Carlo simulation and illustrates the triangular and normal distributions for the input parameters and the normal distributions for the outputted FoS values. Figure 6 displays an illustration of a normal distribution of outputted FoS showing the probability of failure defined as the percentage of FoS values < 1.0.

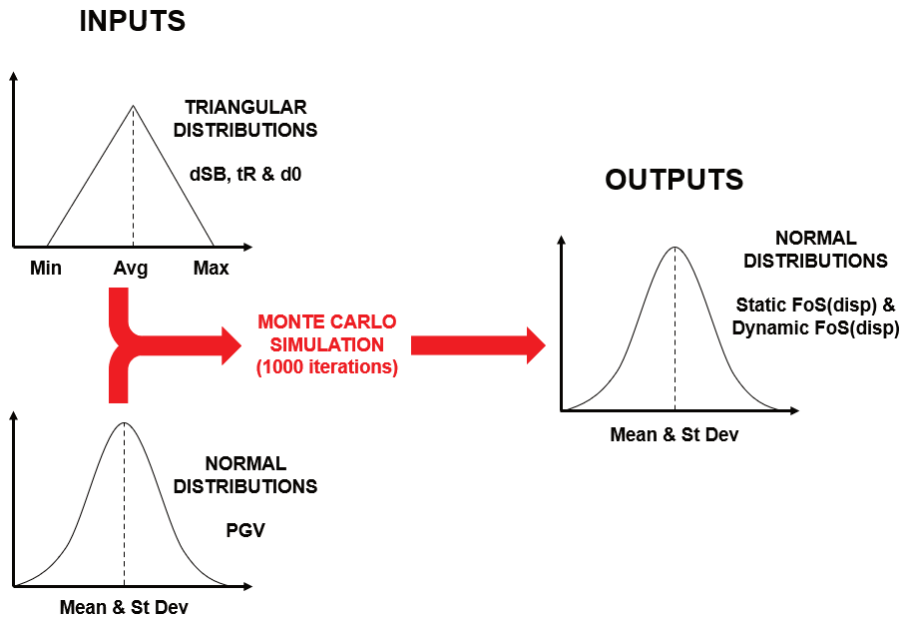

Figure 5 Process map for the probabilistic approach showing triangular and normal distributions for the input parameters and normal distributions for the output FoS values

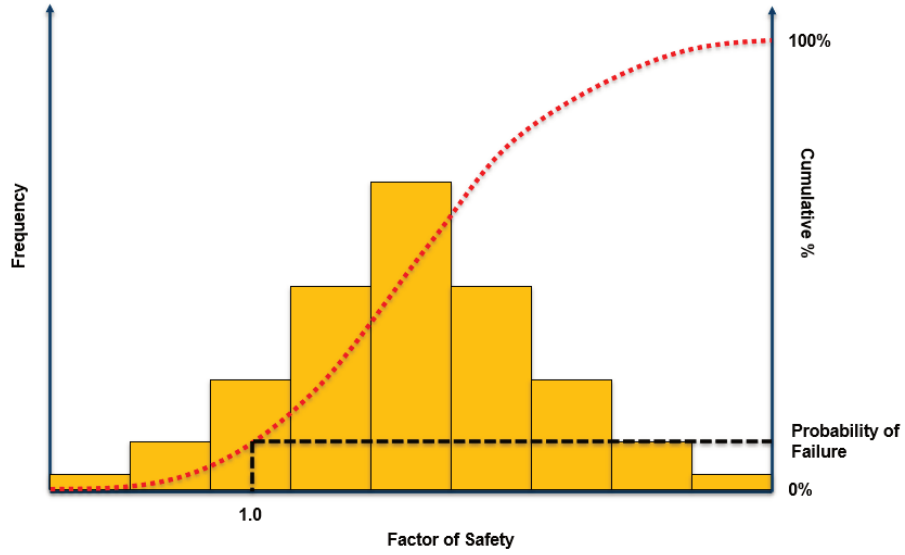

Figure 6 Normal distribution for FoS showing the probability of failure defined as the percentage of FoS values less than 1.0

This definition of failure and Pf is conservative in the sense that the 'failure' definition does not account for the fact that a support system typically retains some support capacity when deformed beyond this state. If the displacement demand is equal to the displacement capacity, the ground support does not necessarily collapse, it has reached the design criteria and is damaged.

2.3 Layers of protection analysis

The layers of protection analysis (Dowell 1997) is a method used across numerous industries to determine the probability of an unwanted event occurring. The underlying concept is that there are numerous controls called independent protection layers (IPLs) that can be used simultaneously to safeguard against an unwanted event occurring. In mining, IPLs are commonly referred to as critical controls. An IPL or critical control is a barrier that can prevent a scenario from cascading to an unwanted event without being adversely affected by either the initiating event or by the action (or inaction) of other IPLs used in the scenario.

The LOPA calculation allows the comparison of quantitative values for the risk of the unwanted event occurring with the risk tolerance values recommended by the Newcrest Process Safety Group. The LOPA calculation is defined by Equation 9:

$$F_i^c = F_i^I \times PFIL_{i1} \times PFIL_{i2} \times \ldots\ldots \times PFIL_{ii} \quad (9)$$

where:

F_i^C = frequency of the consequence for scenario i.

F_i^I = frequency of the occurrence of the initial event.

$PFIL_{ii}$ = probability of failure of an IPL for scenario i.

IPLs used in the ground support assessment include the following:

- The frequency of occurrence of the remote triggering seismic event (design event).
- The effectiveness of blast exclusion zones following an undercut or drawbell blast.
- The probability of failure of the ground support as determined by the probabilistic displacement-based approach.
- The effectiveness of the Short-Term Activity Tracker (STAT) system which alerts the Site Asset Operations Centre and on-call geotech personnel to a heightened seismic activity rate in specific parts of the mine invoking temporary exclusion zones until the seismicity has subsided.
- The occurrence of personnel on foot and not protected by a Falling Objects Protection System (FOPS) cabin.

For the example described in this paper, the risk of the unwanted event (i.e. the LOPA acceptance criteria) of a strainburst breaching the ground support and exposing personnel to a rockfall was set as being less than 1×10^{-5}. It is important to note that in the LOPA assessment the effectiveness of the ground support is one of several IPLs, all playing a role in interrupting the sequence of events that could eventually result in a rockfall related fatality. Table 1 shows the LOPA IPLs (critical controls) and their respective probability of failure values for personnel working in the undercut level.

Table 1 Layers of protection analysis independent protection layers and their respective probability of failure values relevant to personnel working in the undercut level

Independent protection layer	Probability of occurrence/failure	Rationale
Probability of design event (Log P 2.0 @20m)	0.0192	Number of design events (Log P > 2.0) per established drawbell
Probability of blast exclusions failure	0.266	Number of events ML > 0.0 that occurred outside of the blast exclusion time
Probability of STAT system failure	0.2	Number of events ML > 0.0 that occurred outside of the blast exclusion time and were missed by the STAT system
Probability of personnel of foot	0.2	The mean time personnel spent outside of a FOPS cabin per established drawbell
LOPA for UDD Drive (excluding ground support)	0.000204	

3 Input parameters

The key input parameters including depth of strainburst (dSB) versus SL, bulking time (tR), pre-existing bolt head displacement (d0) and PGV were all back analysed using site data.

3.1 Depth of strainburst versus stress level

The depth of strainburst (dSB) is directly related to how much stress the rock is subjected to relative to the strength of the rock through the SL, as defined by Equation 10. Back-analysis using numerical modelling allowed observed depth of strainbursts to be correlated to the SL present at the excavation. Table 2 shows the three SL domains and associated dSB values derived from the back-analysis. The back-analysis showed that for SL values less than 0.4, no strainbursting is observed. For SL values between 0.4 and 0.85, strainbursts between 0.2 m deep and 1.0 m deep are observed. For SL values greater than 0.85, strainbursts between 0.2 m deep and 1.5 m deep are observed.

The SL is the in-plane tangential stress conditions present at the excavation and is defined by Equation 10:

$$SL = \frac{(3\sigma_{1ip} - \sigma_{3ip})}{\sigma_c} \quad (10)$$

where:

- σ_{1ip} = major principal stress in the plane (MPa).
- σ_{3ip} = minor principal stress in the plane (MPa).
- σ_c = uniaxial compressive strength of the intact rock (MPa); typically use upper 75th percentile of standard UCS test data unless Equation 10 has been calibrated on depth of failure data.

Table 2 Depth of strainburst (dSB) versus stress level domains from the numerical modelling back-analysis

Domain	Stress level	dSB range	Distribution
Low	0 to 0.4	Zero	n/a
Moderate	0.4 to 0.85	0.2 m (lowest) 0.4 m (mean) 1.0 m (highest)	Triangular
High	0.85 to 1.3	0.2 m (lowest) 0.8 m (mean) 1.5 m (highest)	Triangular

3.2 Bulking time

The time taken for the strainburst damage to occur (bulking time) was back analysed from the seismic data captured from damaging strainburst events using the procedure described by Malovichko & Kaiser (2020) and Kaiser & Malovichko (2022). Table 3 shows the resulting bulking times for damaging strainburst events at Cadia. The time taken for the strainbursts to bulk is between 30 ms and 50 ms.

Table 3 Back analysed bulking times

Domain	Deformation time (tR) range	Distribution
All	1/20 sec (50 ms) – lowest 1/25.3 sec (39.5 ms) – mean 1/33 sec (30 ms) – highest	Triangular

3.3 Pre-existing bolt head displacement

The pre-existing bolt head displacements were back analysed from site SMART cable data and Lidar scans. SMART cables set in areas exhibiting the onset of Level 3 damage (Lidar scan wall convergence of 80 mm) based on the Cadia Excavation Management TARP (2018) were interrogated to determine the displacement registered. The back-analysis showed that the cables and rockbolts had stretched between 27 mm and 50 mm in these areas as shown in Table 4.

Table 4 Back analysed pre-existing bolt head displacement

Domain	d_0 range	Distribution
All	27 mm (lowest) 37 mm (mean) 50 mm (highest)	Triangular

3.4 Design seismic event

The design seismic event was determined from ground motion prediction equations derived from Cadia seismic data (Mendecki 2021). During the undercutting phase, the design seismic event is considered a log P 2.0 at 20 m producing a mean PGV of 0.82 m/sec with a standard deviation of 0.1 m/sec. This design event applies to the excavations directly related to the undercutting process and includes extraction drives, drawpoint drives, and undercut drives. Table 5 shows the design seismic event and relevant PGV ranges during the undercutting phase.

Table 5 Design seismic events and associated PGV ranges

Phase	Applicable excavations	Design seismic event	PGV range	Distribution
Undercutting	Extraction drives Drawpoint drives Undercut drives	Log P 2.0 event @ 20 m	0.82 m/sec (mean) 0.10 m/sec (std dev)	Normal

3.5 Ground support systems capacities

The ground support systems assessed consist of various combinations of four support elements. These include fibre-reinforced shotcrete (FRS), Minax mesh, 20 mm diameter Posimix bolts, and 17.8 mm diameter single strand cables. Table 6 shows the support element capacities while Table 7 shows the three different ground support profiles assessed for the EXT drive. Because this is a 'local' assessment, only the individual bolt capacities were considered.

Table 6 Bolt element support capacities

Support type	Element	Bonding	Average load capacity	Energy capacity
Primary	20 mm diameter Posimix Bolts (2.4 m long)	1.4 m de-bonded	235kN @ 130 mm (DSI 2017)	30.6 kJ @ 130 mm
Secondary	17.8 mm, plain, single strand cable bolts (4.5 m long)	Fully grouted	320kN @ 75 mm (Kusui 2021; PK Kaiser 2021, pers. comm.)	24.0 kJ @ 75 mm

Table 7 Support profiles assessed for the EXT drive

Support element	GS01	GS02	GS03
FRS	50 mm	50 mm	50 mm
Mesh	Minax	Minax	Minax
Posimix bolt and ring spacing (m)	1.5 × 1.5m	1.3 × 1.3m	1.5 × 1.5m
Cable bolt and ring spacing (m)	–	–	1.5 × 1.5m
Bulking factor	5.8%	5.3%	4.4%

4 Results

4.1 Probability of failure assessment

Table 8 shows the resulting probabilities of failure for the three ground support profiles assessed. The lightest ground support system (GS01) has the highest bulking factor and hence the largest probabilities of failure. The heaviest ground support system (GS03) has the lowest bulking factor and hence the lowest probabilities of failure.

Table 8 Probabilities of failure for the strainburst mechanisms

Failure mechanism	GS01	GS02	GS03
Local dynamic during strainburst	13.79%	2.97%	2.39%
Local static after strainburst	5.46%	1.28%	0.71%

4.2 Layers of protection analysis assessment

To produce the final probabilities of the unwanted event of a person being exposed to a strainburst event that breaches the ground support, the LOPA value excluding ground support of 0.000204 (as derived in Table 1) for the UDD drive is simply multiplied by the probabilities of failure for each ground support profile. Table 9 shows the resulting probabilities of the unwanted event for each ground support profile assessed.

Table 9 Final layers of protection analysis probabilities of the unwanted event of a person being exposed to a strainburst event breaching the ground support

Failure mechanism	GS01	GS02	GS03
Local dynamic during strainburst	2.82×10^{-5}	6.06×10^{-6}	4.89×10^{-6}
Local static after strainburst	1.12×10^{-5}	2.62×10^{-6}	1.44×10^{-6}

The results show that based on the local static and dynamic FoS($_{disp}$), ground support profile GS01 does not meet the LOPA acceptance criteria of 1×10^{-5} and subsequently should not be used to support the UDD excavation. Ground support profiles GS02 and GS03, however, both meet the LOPA requirement. Hence the UDD excavation could be adequately supported using GS02 comprising 50 mm FRS, Minax mesh, and Posimix bolts at 1.3 × 1.3m spacings. While the heavier support profile of GS03 also meets the LOPA requirement, the addition and subsequent expense of cables at 1.5 × 1.5 m is not required for the design case considered but may be required for other failure mechanisms such as shakedown. Such other failure mechanisms also need to be assessed.

5 Conclusion

The paper describes the probabilistic, displacement-based methodology used for Cadia which is based on the approach developed by Kaiser (2020a, 2020b), Kaiser & Moss (2022) and Moss & Kaiser (2022). The method shown is for the local or individual bolt assessments under a dynamically loaded strainburst scenario. To adequately capture the variability of the input data, a probabilistic approach was used where the inputs were represented by either triangular or normal distributions. The assessment was performed using a Monte Carlo simulation where 1,000 calculations were performed for each ground support profile assessed. The outputs of the analysis, which included the local dynamic FoS during the strainburst and the local static FoS after the strainburst were represented as normal distributions. The probabilities of failure for each output were determined as the percentage of FoS values less than 1.0.

The probabilities of failure for each ground support profile were then applied to a LOPA in which other controls, in conjunction with the ground support, were considered. These included the occurrence of the design seismic event, the effectiveness of blast exclusions, the effectiveness of the STAT system, and the occurrence of personnel on foot (not protected by a FOPS cabin). For the example shown, the acceptable probability of the unwanted event of a person being exposed to a strainburst event that breaches the ground support was set at 1×10^{-5}.

The benefits of this approach are that the variability of the input data is adequately captured in the calculations, a large range of resulting factors of safety are considered to determine the probability of failure of each support profile assessed, and several controls are considered other than the ground support to reduce the probability of a person being exposed to a strainburst event that breaches the ground support.

This paper did not consider an assessment of the overall support system capacities, nor did it consider the static loading and shakedown potential before or after the strainburst events. Static and shakedown assessments post the strainburst events are an important consideration for ground support design as the deformed support must be able to contain both the static loads and the shakedown loads from the PGV once the strainburst volume has formed. For a complete assessment of the ground support profiles, these mechanisms need to be considered.

Acknowledgement

The authors acknowledge Peter Kaiser for his invaluable work in developing the displacement-based ground support approach and guiding its implementation at Cadia. The authors also thank Newcrest Mining for allowing the publishing of this paper.

References

Cadia Excavation Management TARP 2018, *Underground Excavation Management for Geotechnical Engineers 730-200-GE-STR-0007*, Newcrest internal document.

Dowell, AM 1997, 'Layer of protection analysis: a new PHA tool, after HAZOP, before fault tree analysis', *International Conference and Workshop on Risk Analysis in Process Safety*, presentation.

DSI 2017, *DSI underground product offering for Newcrest Cadia Valley Operations*, Newcrest internal document.

Kaiser, PK 2020 a, *Newcrest Support Design Handbook 200712*, Newcrest internal consultant report from GeoK Inc.

Kaiser, PK 2020b, *Dynamic Support System Design (DSSD) Tool*, Microsoft Excel calculator developed for Newcrest.

Kaiser, PK & Moss, A 2022, Deformation-based support design for highly stressed ground with a focus on rockburst damage mitigation', *Journal of Rock Mechanics and Geotechnical Engineering*, vol. 14, no. 1, pp. 50–66.

Kaiser, PK & Malovichko, D 2022, 'Energy and Displacement Demands Imposed on Rock Support by Strainburst Damage Mechanisms', *RASIM10*, Society for Mining, Metallurgy & Exploration, Tucson.

Kaiser, PK, Tannant, DD & McCreath, DR 1996, *Canadian Rockburst Support Handbook*, Geomechanics Research Centre, Laurentian University, Sudbury.

Kusui, A 2021, *Results from Dynamic Testing of 15.2 mm and 17.8 mm Diameter Cable Bolt Reinforcement Systems 730-200-GE-MEM-0066*, Newcrest internal memorandum.

Lowther, R 2017, *Strategy for geotechnical control of near-field mine excavations at Cadia East post 14th April 2017 Seismic Event*, Newcrest internal memorandum.

Malovichko, D & Kaiser, PK 2020 'Dynamic model for seismic shakedown analysis', *Proceedings of the 54th US Rock Mechanics/Geomechanics Symposium*, American Rock Mechanics Association, Alexandria.

Mendecki, A 2021, *Simple GMPE for Cadia East Mine*, Newcrest internal consulting report from IMS.

Morissette, P, Hadjigeorgiou, J & Thibodeau, D 2011 'Assessment of support performance under dynamic loads at Vale Creighton Mine', *Proceedings of the 45th US Rock Mechanics/Geomechanics Symposium*, American Rock Mechanics Association, Alexandria.

Morissette, P, Hadjigeorgiou, J & Thibodeau, D 2012, 'Validating a support performance database based on passive monitoring data', in Y Potvin (ed.), *Deep Mining 2012: Proceedings of the Sixth International Seminar on Deep and High Stress Mining*, Australian Centre for Geomechanics, Perth, pp. 27–39, https://doi.org/10.36487/ACG_rep/1201_02_morissette

Moss, A & Kaiser, PK 2022, 'An operational approach to ground control in deep mines', *Journal of Rock Mechanics and Geotechnical Engineering*, vol. 14, no. 1, pp. 67–81.